J Ther Eng, Vol. 10, No. 5, pp. 1149−1163, September, 2024

Journal of Thermal Engineering
Web page info: https://jten.yildiz.edu.tr
DOI: 10.14744/thermal.0000858

Research Article

Thermal analysis of photovoltaic-thermoelectric hybrids

Rida Y. NUWAYHID[1,*], Mohamad S. RAHAL[1], Yamen Z. MAKAREM[2], Roger R. ACHKAR[1]

[1]*Faculty of Engineering, American University of Science and Technology, Beirut, 16-6452, Lebanon*
[2]*Department of Energy and Processes Engineering, Technical University of Berlin, 10117, Germany*

ARTICLE INFO

Article history
Received: 08 August 2023
Revised: 23 October 2023
Accepted: 25 October 2023

Keywords:
Efficiency; Figure-of-Merit; Hybrids; Photovoltaics; Solar; Temperature; Thermoelectrics

ABSTRACT

There continues to be considerable research on the adverse effect of photovoltaic (PV) panel temperature on its power production. Aside from attempting to minimize heating up of the panel by providing heat sinks and the like, several studies looked into using the unconverted heat as an input to a Thermoelectric generator residing below the PV panel and questionably generating additional power. Using simple steady energy balances, simplified steady thermal models of PV panels, individually or thermally-in-series coupled to heat engines are studied. The nodal energy equations are solved to ascertain resulting temperatures and efficiencies under different insolations. After establishing a simplified model for a lone PV panel, a PV panel with an added thermoelectric generator attached to its back side is studied. Solving the associated steady energy equations, the photovoltaic-thermoelectric system is found to have a smaller than expected advantage in net power, no more than 4.15 %, over the lone PV panel and then only at high insolation's and concentrations. The implication of this work is that hybridizing a PV panel by bottoming it with a thermoelectric generator is not quite attractive except possibly at higher solar concentrations. The margin to Increase the overall efficiency of a photovoltaic-thermoelectric hybrid by improving the thermoelectric-figure-of-merit does not appear to be significant although further consideration of thermoelectric materials may be required.

Cite this article as: Nuwayhid RY, Rahal MS, Makarem YZ, Achkar RR. Thermal analysis of photovoltaic-thermoelectric hybrids. J Ther Eng 2024;10(5):1149−1163.

INTRODUCTION

Photovoltaic systems are increasingly proliferating nowadays with a global installed capacity of over 1185 GW and a yearly market of over 240 GW [1]. Since photovoltaic systems are solar-based and use only a specific part of the available input solar flux, output power has been limited with efficiencies rarely exceeding 22% and thus there has been a need to look for higher efficiencies of conversion. The rising trend continues and the current effort is on further development and refinement of the conversion technology as well as a continuation of the search for better energy storage.

As it is well known that arresting the temperature, or even cooling it limits the drop in its efficiency with temperature, prescriptions for "cooling" the PV panel were studied. One research approach is best exemplified by

*Corresponding author.
*E-mail address: rnuwayhid@aust.edu.lb

This paper was recommended for publication in revised form by Editor-in-Chief Ahmet Selim Dalkılıç

Published by Yıldız Technical University Press, İstanbul, Turkey

considering Photovoltaic-thermal (PVT) "hybrid" systems that have both PV cells as well as regular solar water heaters (SWH) in one panel. The study is that of Chavez-Erbiola et al. [2] who considered a standard SWH panel with normal solar input, but however, incorporated transparent PV with Thermoelectric generators (TEG's) embedded below these which are in turn cooled by the circulating working fluid of the solar panel. Additionally, Najafi and Woodbury [3] modeled a PVT air cooled system bottomed by TEG modules and evaluated the results for a summer day in Tuscaloosa, USA. However, they found that the TEG component never generated more than about 2-3% of the total PVT-TEG hybrid output. Clearly this is not a true hybrid but rather a "combined "system since it uses the same input spectrum but in two semi-autonomous devices. Such systems have not proliferated since they are somewhat bulky and somewhat complicated.

Another option was to actually use active cooling and to try and search for feasible conditions. Thus, several studies have attempted to cool the PV panel by using thermoelectric (Peltier) cooling (TEC) modules. For example, Kane and Verma [4] claimed that the PV can be cooled by 10°C without power loss while Benghanem et al. [5] reported that TEC cooling of a PV panel may arrest the 0.5% drop in efficiency per degree rise with no more than a 6% increase in cost. Hadi et al. [6] qualified these results by showing that the power requirements of the TEC's becomes excessively high with larger PV panels. Furthermore, a study by Kayabasi and Kaya [7] experimentally evaluated a Phase Change Material (PCM) placed below a solar PV panel with an added TEG. They clearly stated that, since TEG's have low efficiency, they work best with waste heat sources such that hybridizing a PV panel with TEG's may lead to power enhancement.

Interest then was diverted more towards attempting to find systems that are closer to being hybrids such as Photovoltaic-thermoelectric generators directly-combined systems. While still not "true" hybrids (since a hybrid would be "one system" that combines features of two parent systems!"), Photovoltaic-thermoelectric systems are physically-related as the two have many common features: both are p-n junction devices; both use electromagnetic energy as their input and both can be adapted to a wide range of engineered devices. Sahin et al. [8] made a comprehensive review of photovoltaic-thermoelectric hybrids and delineated the influence of key parameters on their performance. Likewise, Tyagi et al. [9] made a broad review of such hybrids including a discussion of performance optimization as well as possible applications of such devices. Another review of interest is that of Chandel et al. [10] which also contains a general discussion of methods to alleviate photovoltaic cell temperature increase.

As such, photovoltaic-thermoelectric combinations that better utilize the solar input energy spectrum in a given PV system or by designing a system that makes use of the solar input by more than one conversion methodology has been the aim. Manipulating the input solar spectrum itself has been considered in some studies that used a spectrum splitter or filter to break the solar flux into two components, long and short wave, and then make use of each partial spectrum in both a PV as well as a thermally-driven device usually in a side-by side fashion. In this sense, Kraemer et al. [11] outlined a PV-TEG optimizing method that looks into the partitioning of the solar input spectrum between different PV materials and a specific thermoelectric generator. Furthermore, input enhancement has been studied by beefing up the solar input signal such as by using concentrating systems which could be lens-based or parabolic reflecting surfaces. One such system design is that of Yonglian et al. [12] who investigated a solar-based system with a spectrum splitter. The short-wave component is routed to the PV part, while the long wave/thermal part is used as heat input to the TEG that converts this heat energy to electricity. Furthermore, using a 2-dimensioal solar tracking system, Kandil et al. [13] found that a hybrid PV-TEG system constrained to a maximum operating temperature of 85°C and a concentration ratio of 8 produced an increase in power of 43% compared to the individual photovoltaic. As such, a number of researchers have looked into the "integration" of thermoelectric and photovoltaic components in the hope of whether there may be a resulting enhancement of output. The models used were simple, consisting of a PV slab resting over a TEG slab so as to be thermally in series. Von Sark [14], utilizing a limiting parametric study predicted a possible improvement of 8-23% in photovoltaic performance when a thermoelectric generator device resides below it.

In fact, a thermoelectric device is capable of being run either as an engine – producing power, or as a refrigerator – utilizing input power to accomplish cooling (or heating). Conventionally, thermoelectric systems, when in power producing mode are usually dubbed thermoelectric generators (TEG's); and when in a reversed cooling mode become thermoelectric coolers (TEC's). In this work, only heat-fed, power generating thermoelectrics will be considered. Therefore, in order to shorten notations a TEG will henceforth be simply called termed a TE.

Park et al. [15] considered the simple PV-on-TE setup with the intention of investigation of conditions for lossless coupling of the two components. They found, with experimental verification, that with proper selection of TE leg dimensions among other aspects, it is possible to design a hybrid system that surpasses a lone PV system in performance. Lorenzi et al. [16] who considered wide-gap solar cell – thermoelectric coupling and found an efficiency gain of 3.05% for a Perovskite-Bismuth Telluride photovoltaic-thermoelectric hybrid.

Somewhat distinctive, a study by Bjork and Nielsen [17] where performance limits have been considered by considering achievable efficiencies and other known or controllable parameters using simple general rules that govern overall conversion. They found a small margin for performance enhancement. In another study by Bjork and

Nielsen [18], motivated by certain results from the literature that they considered vague, and using an upper bound assumption that the TE's cold side is somehow kept equal to the reference ambient, the study found that such systems were not capable of producing more power than a PV system alone. For example, they suggest that the results of Park et al. [15] or Wang et al. [19] may be suspect of violating the Carnot limit. They did not find any feasible window for simple Photovoltaic-on-Thermoelectric hybridization as they reported mostly negative results. On the positive side, it was also suggested that it may be that these hybrid generator systems may be operating in a unique mode that warrants more study. Lamba and Kaushik [20] studied a detailed analytical modelled of a PV-TE hybrid and found that the efficiency increases by 13.27% at a concentration ratio of 3 (at an insolation of 600 W/m^2). On the same theme, Chandan et al. [21] studied Photovoltaic-thermoelectric hybrids both outdoors and indoor with a solar simulator. Among other results, they found that the indoor results showed that the thermoelectric contribution of the hybrid never exceeded 1% of the total power. Hence, they questioned the value of adding a thermoelectric generator in tandem with a photovoltaic panel. Another select study of relevance to the spectrum splitting route to photovoltaic-thermoelectric coupling is that of Yin and Li [22] who showed that current matching and Peltier effect reduction can lead to output enhancement in a spectrum-split photovoltaic-thermoelectric device.

Given the somewhat unclear and sometimes conflicting status of results and since apparently the greatest doubts appear to be linked to the temperature span across the TE component of a tandem PV-TE hybrid, this study is an attempt to go back to basics and to consider very simple thermal energy balances as well as basic PV and TE theory in order to bound possible results and ascertain whether there is a gain that ensues when a TE is connected thermally in series below a PV. The results of this work appear to indicate little or no gain although further scrutiny is warranted.

METHODOLOGY

The study starts with a simple single (lone) PV panel. A steady 1-dimensional steady thermal energy balance is applied on the panel: first assuming the panel to be represented by one average temperature (1-node method), then a 2-node energy balance is done. This is followed by a comparison of the two models for the PV panel. The motivation for this diversion is to confirm that the simple model may be sufficiently accurate for further studies. The second part of the work starts by adding a heat engine below (in tandem with) the PV panel. This is done again by a setting up a steady 1-dimensional energy balance spanning the PV and the device below it. This starts by assuming a reversible heat engine (a Carnot engine) with hot and cold side temperatures below the PV, then the deliberations introduce an irreversible (a TE below the much-simplified PV panel model. The crux of the work then centers on a model of a 1-node PV panel with incident insolation with a TE thermally below it and represented by two temperature nodes: the hot side adjacent the PV and the cold side that transfers heat to the ambient via a certain heat sink. Besides partial results and discussions within each section, a discussion of the results that directly pertain to the main aim of this work ensues. What follows tackles each step of the mentioned thermal models by simply setting up a steady energy balance and solving the set of nodal equations for the required node temperatures and the effect on power and efficiency.

The Lone PV

Prior to considering any combined or hybrid system, it is quite useful to start by simplifying the modelling of the lone PV slab. Minimal detail, in the simplest, yet sufficiently accurate manner can establish for further system incorporations and complications and provide readily obtainable bounding values with minor loss in accuracy.

Simplest model – 1-node lone PV

The PV slab may be taken to be represented as a closed lumped system with one single temperature T_p. The slab then simply receives heat from above and losses heat to the ambient from both its upper and lower surfaces, viz.,

$$\tau\alpha CGA_P(1-\eta_P) = 2hA_P(T_P - T_a) \tag{1}$$

Here the area for heat loss (A_p) is doubled to account for the exposed bottom loss considering no fins are used. h is the convection coefficient and τ (transmissivity of glass cover) and α (absorptivity of PV material) are used to add some reality to the heat absorbed. The Shockley-Queisser limit [23] continues to give a simple and as yet valid expression for PV efficiency drop with temperature for c-Si type converters.

$$\eta_p = \eta_R\big(1 + \beta_R(T_R - T_P)\big) \tag{2}$$

Where η_R is the references efficiency, T_R is the reference temperature and β_R is the reference temperature-dependent coefficient. The mentioned values for c-Si are taken to be 0.12, 293K and 0.0039K^{-1}, Skoplaki and Palyvos [24], consequently,

Expanding the efficiency term, inserting into the energy balance and solving for T_P:

$$T_P = \frac{1}{1-\dfrac{\tau\alpha CG}{2h}\eta_R\beta_R}T_a + \frac{\dfrac{\tau\alpha CG}{2h}(1-\eta_R(1-\beta_R T_R))}{1-\dfrac{\tau\alpha CG}{2h}\eta_R\beta_R} \tag{3}$$

The resulting expression for the efficiency as a function of only ambient and device-dependent parameters would then be:

$$\eta_P = \frac{\eta_R(1+\beta_R T_R) - \frac{\tau\alpha CG}{2h}\eta_R\beta_R(1+2\eta_R\beta_R T_R)}{1-\frac{\tau\alpha CG}{2h}\eta_R\beta_R} - \frac{\eta_R T_R}{1-\frac{\tau\alpha CG}{2h}\eta_R\beta_R}T_a \quad (4)$$

Figure 1 shows the PV temperature for different insolation and concentration levels. Figure 2 further reveals that with no concentration (C=1), at a given heat loss coefficient and ambient, the PV efficiency drops slightly. As concentration is increased, the panel efficiency increasingly drops as a result of the high PV temperature. In such cases, the usual suggested practice was to add extended surfaces or phase change material (PCM) packs on the back side of the panel in order to reject or capture the non-converted heat that is responsible for the PV's temperature rise. This is a highly critical situation as it is seen that at a concentration of 4 (an easily achieved value) with an insolation of 1000 W/m^2, the panels temperature can reach 85°C and its efficiency drops to around 9%.

More detailed model – 2 node lone PV

Adding detail into the simple PV model could start by assuming the slab to have an upper T_{p1} and lower T_{p2} temperature rather than one temperature. However, the PV extracted power will have to be assumed to be removed at

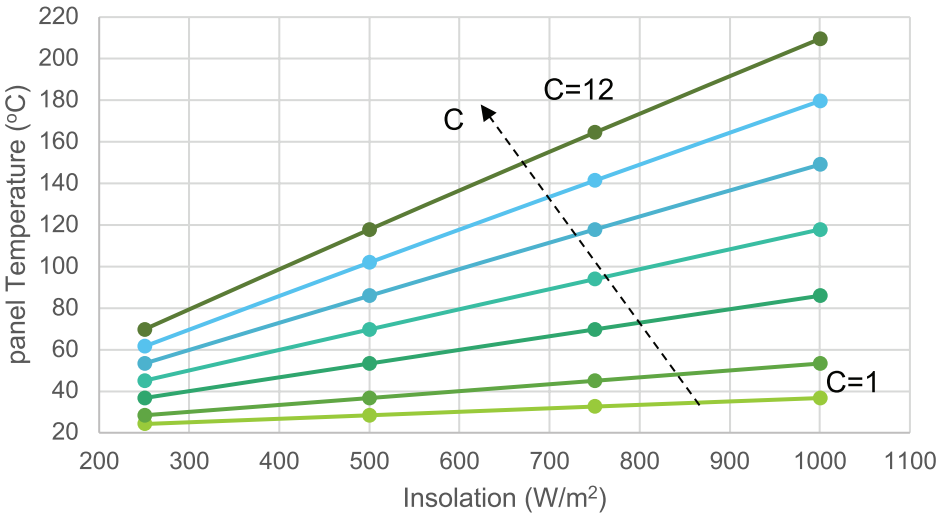

Figure 1. Lone 1-node PV panel temperature as a function of insolation at increasing concentrations (C=1,2,4,6,8, 10 and 12) as the arrow direction indicates (T_a=25°C, h=22 W/m^{2}K).

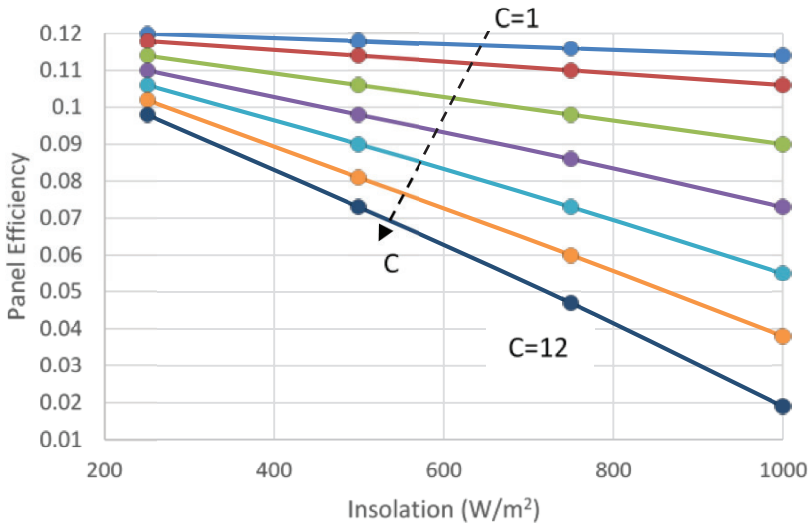

Figure 2. Lone 1-node PV panel efficiency as a function of insolation at increasing concentrations (C=1,2,4,6, 8, 10, and 12) as the arrow direction indicates (T_a=25°C, h=22 W/m^{2}K).

Table 1. Realistic layer properties and thicknesses of typical PV panel

Layer	Layer material	Thickness, Li (m)	Density, ρi (kg/m³)	Thermal Conductivity ki (W/m.K)	Specific Heat, Ci (J/kgK)	Li/ki
1	Glass	0.003	3000	1.8	500	0.001667
2	ARC	1.00E-07	2400	32	691	3.13E-09
3	PV	2.25E-04	2330	148	677	1.52E-06
4	EVA	5.00E-04	960	0.35	2090	0.001429
5	Rear Contact	1.00E-05	2700	237	900	4.22E-08
6	Tedlar	1.00E-04	1200	0.2	1250	0.0005
Sums		0.00383				0.003597

one node – in this study it will be the upper node although a 3-node model would be better. Furthermore, here a heat-sink effectiveness (ε) will be assigned to the lower surface to allow for extended surface heat loss enhancement if so desired. With 2 nodes, the thermal conductivity of the PV comes into play and therefore needs to be determined. The PV is thus given an "effective thermal conductivity" by conserving heat flux through its actual multilayers as evaluated by Equation 5. For the typical values in Table 1, the effective k is about 1.07 W/m.K.

$$k_{eff}^{PV} = \frac{\sum_i L_i}{\sum_i \left(\frac{L}{k}\right)_i}, \tag{5}$$

The energy balances at the two surfaces: upper (T_{p1}) and lower (T_{p2}) are:

$$\tau\alpha CG A_P(1-\eta_P) = hA_P(T_{P1}-T_a) + \frac{k_p}{L_p}A_p(T_{p1}-T_{p2}) \tag{6}$$

and,

$$\frac{k_p}{L_p}A_p(T_{p1}-T_{p2}) = \varepsilon h A_P(T_{P1}-T_a) \tag{7}$$

The insertion of the Shockley-Queisser [23] relation for the PV efficiency gives the temperatures as:

$$T_{P1} = \frac{1+\varepsilon}{1+\varepsilon-\frac{\tau\alpha CG}{h}\eta_R\beta_R}T_a + \frac{\frac{\tau\alpha CG}{h}(1-\eta_R(1-\beta_R T_R))}{1+\varepsilon-\frac{\tau\alpha CG}{h}\eta_R\beta_R} \tag{8}$$

and

$$T_{p2} = \frac{1+\varepsilon\left(1-\frac{L_p}{k_p}\tau\alpha CG\eta_R\beta_R\right)}{1+\varepsilon-\frac{\tau\alpha CG}{h}\eta_R\beta_R}T_a + \frac{\left(1-\varepsilon\frac{hL_p}{k_p}\right)\left(\frac{\tau\alpha CG}{h}(1-\eta_R(1-\beta_R T_R))\right)}{1+\varepsilon-\frac{\tau\alpha CG}{h}\eta_R\beta_R} \tag{9}$$

So that the PV slab has an average temperature of:

$$\tilde{T} = \frac{1+\varepsilon\left(1-\frac{L_p}{2k_p}\tau\alpha CG\eta_R\beta_R\right)}{1+\varepsilon-\frac{\tau\alpha CG}{h}\eta_R\beta_R}T_a + \frac{\left(1-\varepsilon\frac{hL_p}{2k_p}\right)\left(\frac{\tau\alpha CG}{h}(1-\eta_R(1-\beta_R T_R))\right)}{1+\varepsilon-\frac{\tau\alpha CG}{h}\eta_R\beta_R} \tag{10}$$

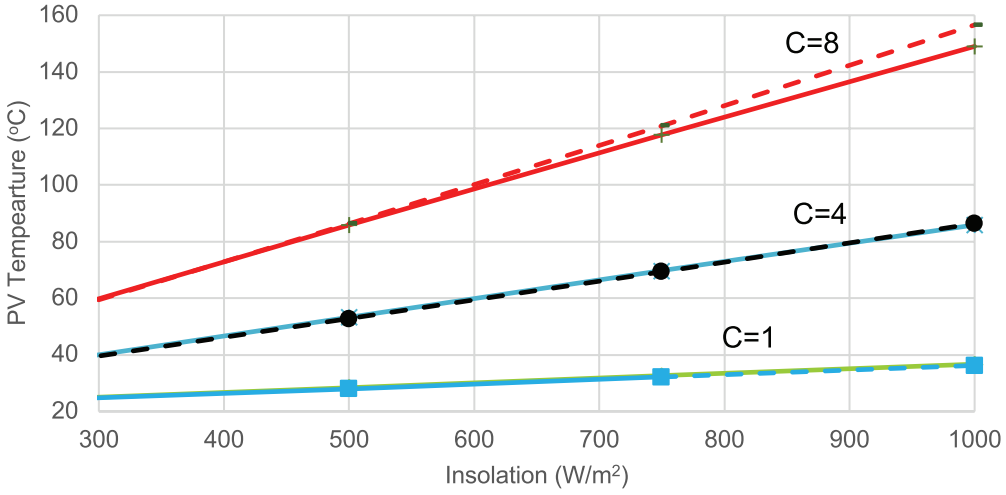

Figure 3. Comparison of PV temperature by 1 node (solid lines) and 2 node (dashed lines) models for 3 concentrations.

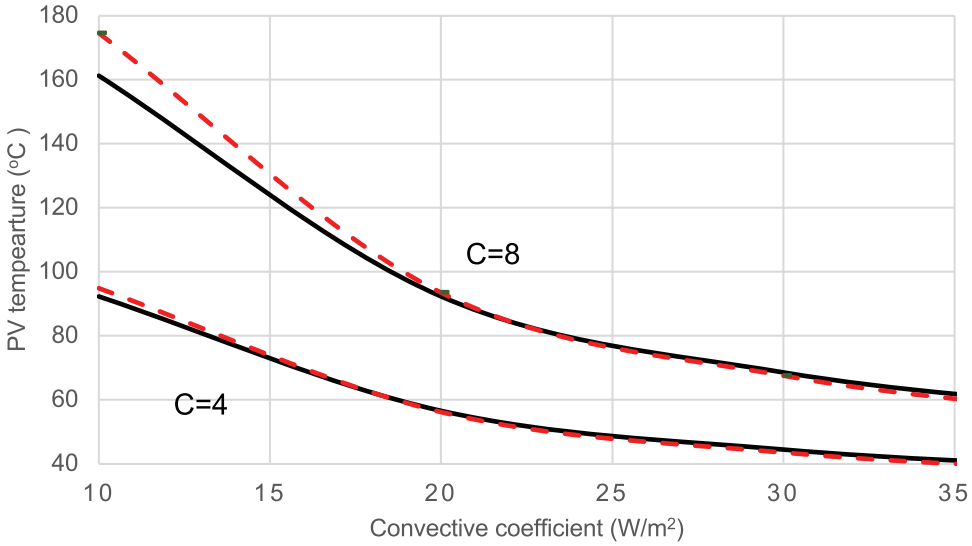

Figure 4. PV temperature dependence on convection coefficient at two different solar concentrations: 1-node model - solid lines and 2-node model - dashed lines.

Figure 3 compares the temperature of the PV slab using the 1-node model with the average temperature using the 2-node model with h=22 W/m²K and an ambient of 20°C. Insolations of 250 to 1000 W/m² as well as solar concentration ratios of 1 to 8 are considered. For clarity, the panel is taken not to have any extended surfaces (ε=1) here.

It is seen that only at high concentration (and low convective coefficients) does the 1 node model slightly underestimate the temperature and hence overestimate the efficiency.

A critical parameter is the convective heat transfer coefficient (assuming it dominates) – Figure 4 shows that at sufficiently large h (considering natural convection only), a 1-node model is quite sufficient. The value being used in this study is 22 W/m²K, which is the winter recommended average convective heat transfer value and is sufficiently large for the 1-node model to be reasonable as the figure shows.

It is therefore judged that because: the PV slab is very thin, the influence of its thermal conductivity not large, and with sufficiently large convection heat transfer, the use a simple 1 node PV model in further studies is justified and is henceforth used in more complex hybrid models.

PV-heat Engine Hybrids

The inescapable rise in temperature of the PV panel, when exposed to higher insolation's inherent with added concentration, overwhelms any increase in efficiency. As such, the non-converted heat has to be either removed (say by extended surfaces) or else dealt with in some other effective manner. Aside from material research into photovoltaic conversion (improving spectral responsivity for example), PV performance improvement could be influenced by marrying the PV slab with a "heat engine"- a device that takes heat (from the PV in this case) and as heat traverses it, further power is extracted. Henceforth, the PV slab is taken to be connected thermally in series with a heat engine that is located on its non-exposed side. Using applied thermodynamics terminology, the heat engine is considered to be "bottoming" the PV slab.

The Carnot-PV hybrid

Theoretically and as an ideal limiting view that puts an upper cap on performance, a "Carnot engine" is taken as the ultimate bottoming heat engine. Having shown it to be sufficient, a 1-node model of a PV slab is used. Thus, the illuminated PV slab with a temperature T_P rejects heat below to a Carnot engine whose hot side is likewise T_P. Furthermore, since an upper bound is being sought anyway, the Carnot engine is taken to reject heat to the ambient at T_a. As such, applying the Carnot principles [25]:

$\eta_c = 1 - \frac{T_a}{T_p}$, or since T_a and the Carnot efficiency (η_C) are fixed, $T_P = \frac{T_a}{1-\eta_c}$

The heat rate rejected to the Carnot engine is that which is not convected away nor converted and is given by:

$$\dot{Q}_{Hc} = CGA_P(1 - \eta_P) - hA_P(T_P - T_a) \quad (11)$$

Where again η_P is a function of T_p through the Shockley –Queisser relation for c-Si. Eliminating T_P in favor of T_a gives:

$$\frac{\dot{Q}_{Hc}}{A_p} = CG(1 - \eta_R(1 + \beta_R T_R)) + \frac{\eta_R \beta_R CG - h\eta_C}{1 - \eta_C} T_a \quad (12)$$

Since $\dot{W}_C = \eta_C \dot{Q}_{HC}$, the specific power contribution from the Carnot engine is:

$$\frac{\dot{W}_C}{A_P} = CG\eta_C(1 - \eta_R(1 + \beta_R T_R)) + \frac{\eta_C}{1 - \eta_C}(\eta_R\beta_R CG - h\eta_C)T_a \quad (13)$$

While the specific power contribution from the PV panel is:

$$\frac{\dot{W}_P}{A_P} = CG\eta_R(1 + \beta_R T_R) - \frac{\eta_R\beta_R CG}{1 - \eta_C}T_a \quad (14)$$

Therefore, the total specific power of the system is:

$$\frac{\dot{W}_T}{A_P} = CG(\eta_c + (1 - \eta_c)\eta_R(1 + \beta_R T_R)) - \left(\eta_R\beta_R CG + h\frac{\eta_C^2}{1 - \eta_C}\right)T_a \quad (15)$$

Using typical c-Si values [24], an ambient of 293K, C=1 and h=22 W/m^{2}K, the specific power outputs are evaluated. Figure 5 shows the total specific power of the PV-Carnot bottomed device which apparently has a clear maximum that lies at low Carnot efficiently values.

This behavior is due to the fact that to obtain high Carnot efficiencies would implicitly suggest higher temperatures such that the more productive PV component would suffer due to these temperatures while the Carnot component would still not be able to compensate. Furthermore, the PV power drops linearly with Carnot efficiency but remains the greater contributor. The figure also shows the enhancement in total power has a maximum that shifts to higher Carnot efficiency values as the insolation increases and clearly at lower insulations and hence lower temperature the Carnot engine produces very little power (lower curve). At an insolation of 800 W/m^2, at a Carnot efficiency of just above 5%, the Carnot engine is at its best but only contributes 18.4% of the total power while the PV panel dominates the output. At lower insolation's, the role of the Carnot engine obviously gets increasingly less.

Bjork and Nielsen [18] did make use of the Carnot limit in conjunction with a thermoelectric generator and found that a combined PV-TE that is assumed to approach the Carnot limit can at best add only 4.5% to the performance of a lone PV cell. Since highly hypothetically, they showed that it is very doubtful that performance could be improved by thermally combing a PV with a highly efficient heat engine in series. This work appears to be in line with that of Bjork and Nielsen and appears to indicate that, in steady-state operation, there is a small window on the possible enhancement of PV output but only at higher insolation's or concentrations. For comparison purposes using the 1-node lone PV alone model, the output power of the lone PV per unit area can be evaluated by:

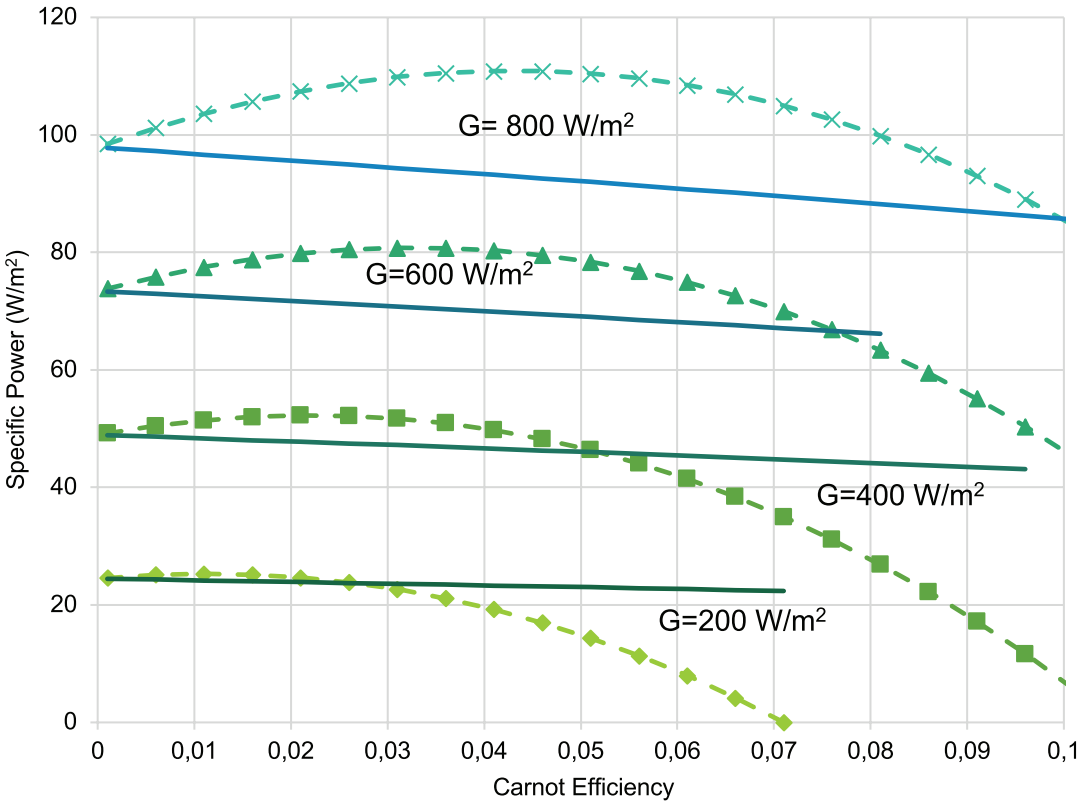

Figure 5. PV power (solid lines) and total (PV + Carnot) power (dashed lines) at 4 different insolation's.

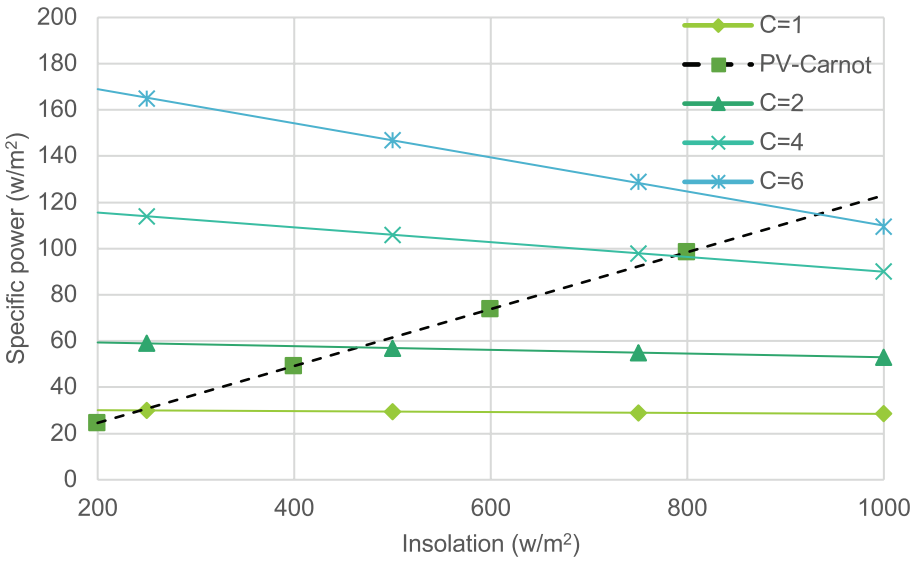

Figure 6. Specific power vs insolation for lone PV (at C=1,2, 4 and 6) compared to PV-Carnot combination at C=1.

$$\frac{W_{PV-alone}}{A_P} = G\frac{\eta_R(1+\beta_R T_R) - \frac{\tau\alpha CG}{2h}\eta_R\beta_R(1+2\eta_R\beta_R T_R)}{1-\frac{\tau\alpha CG}{2h}\eta_R\beta_R} - \frac{\eta_R T_R G}{1-\frac{\tau\alpha CG}{2h}\eta_R\beta_R}T_a \quad (16)$$

Figure 6 shows the specific power of a PV-Carnot hybrid as evaluated by Equation 15 at C=1 and is seen to generate more power as the insolation increases. On the other hand, lone PV cases are shown for C=1, 2, 4 and 6 which show a slow decrease in power with insolation as expected from the associated rapidly rising temperature and can only compete with PV-Carnot device at high and costly concentrations – but then only up to the temperature-dependent material limit of the PV material (normally about 250°C). While a hypothetical Carnot engine was used here, it nevertheless is helpful in showing that at higher insolation's adding a heat engine can make a difference although this may not be very significant. While the observed margin appears small, a more realistic bottoming of the PV using an irreversible heat engine such a TE may provide more insight.

The TE bottomed PV

While a Carnot engine is unrealizable and only serves as an upper ceiling, a more realistic heat engine would be one that has internal irreversibility's in its operation. The Thermoelectric heat engine thus serves as a more doable system since it is inherently internally irreversible. Thus, putting aside any external irreversibility's associated with heat transfer to/from our system(s), and in-line with many researcher's, the thermoelectric generator serving as a bottoming engine to the Photovoltaic generator is considered in order to ascertain if such a marriage may be fruitful in a steady operating regime.

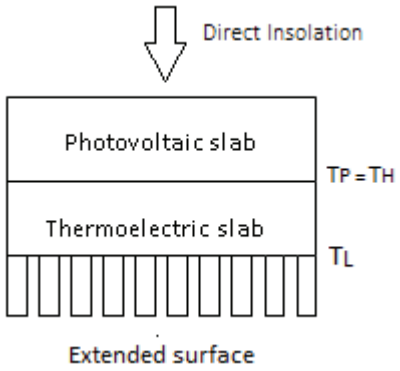

Figure 7. The 1-node PV slab bottomed by a TE slab with a heat sink of effectiveness ε.

Bottoming the PV by a TE is actually possible although as mentioned before results of several research papers appear to be giving different results and more importantly do not give a definitive answer on whether such an action is thermally feasible. This question may be posed somewhat like the question of whether a PV bottomed by a TEC (note the "C") is feasible – clearly no! The best TEC barely reaches a COP of 1.0 which therefore means it will not be able to cool the PV sufficiently without consuming more power in steady operation than the PV produces.

A simple PV slab, with a given thermal conductivity has a simple TE slab residing below it – such an assembly is from herein forth called a TE-bottomed-PV slab. The PV slab is exposed from above to solar illumination and losses heat at its surface (Fig. 7). The PV slab transmits the unconverted heat to the TE slab below it via conduction, which in turns transmits unconverted heat and "convects" it to the surroundings from below through a finned heat sink. Heat

loss by radiation is simply included by incorporating it in a combined coefficient.

Assuming negligible thermal contact resistance both at the PV-TE interface and between the TE and the heat sink, similar cross-sectional areas, similar heat transfer coefficients, the steady energy balances across the PV-TE slab are written and solved using the simple 1-node PV model – first assuming heat rejection from the device at T_a then at the higher and more realistic temperature T_C.

Simple one–node PV-TE model

Considering that the PV slab is very thin, it is sufficient to analyze it using a single node with one average temperature. Hence, it is assumed that the TE below has a hot side temperature equal to the PV temperature T_p.

A steady energy balance on the thin PV strip states that the input absorbed solar energy is balanced by the energy leaving as heat losses to the ambient from above plus the converted electric energy and the residual waste heat that is available to the TE below as an input, viz.:

$$\tau\alpha CGA_P = hA_P(T_P - T_a) + \tau\alpha CGA_P\eta_p + \dot{Q}_H \qquad (17)$$

Hence the rate of residual heat per PV area (A_p) that is transferred to the thermoelectric strip on the bottom is:

$$\frac{\dot{Q}_H}{A_P} = CG(1 - A) - (BCG - h)T_P + hT_a \qquad (18)$$

Where, as before, use has been made of the Shockley-Queisser [23] expression for C-Si (equation with A=0.2595 and B=0.000468 K^{-1} Concentration values include absorptivity and transmissivity are accounted for in the insolation values (such that τ=0.8 and α=0.8)

Taking the cold side of the TE to be at the ambient temperature (T_a) as a first consideration simplifies calculations while providing an upper bound on performance. Neglecting the Thomson effect, the steady rate of heat entering the TE hot junction ($\dot{Q}_H$) is balanced by the heat leaving it by Conduction and by the reversible Peltier less half the heat dissipated in the junction by the joule effect – viz: $\dot{Q}_H = \dot{Q}_{peltier} + \dot{Q}_{Comduction} - \frac{1}{2}\dot{Q}_{joule}$, where the Peltier heat is given by the Peltier Effect $\dot{Q}_{peltier} = 2s_T IT_H$, the conduction heat given by the Fourier Effect $\dot{Q}_{conduction} = \frac{2k_T A_P}{l}(T_H - T_a)$, and the joule effect is given by $\dot{Q}_{joule} = I^2R = I^2\frac{2\rho_T A_L}{l}$. Where s_T, k_T and ρ_T are the Seebeck coefficient (V/K), the thermal conductivity (W/m.K) and the electrical resistivity (Ω.m) of the thermoelectric material (Bismuth Telluride in this case). It has also been assumed that the n and p legs of the thermocouple have nearly equal property magnitudes and therefore the factor 2. In addition, as is commonly assumed, the total joule heat dissipated in the thermocouple is assumed to be equipartitioned between the hot half and the cold half of the couple – hence the one-half factor. Manipulating the above produces:

$$\frac{\dot{Q}_H}{A_P} = \frac{s_T IT_H}{A_L} + \frac{k_T}{l}(T_H - T_a) - \frac{1}{2}I^2\frac{2\rho_T l}{A_L^2} \qquad (19)$$

Where A_L appears after dividing both sides by A_p and noting that each couple has an area of approximately $2A_L$, where A_L is the area of one thermoleg. T_p is equal to T_H in this 1 node treatment.

Sufficient for such a scoping study, the TE may be modelled assuming operation at maximum power conditions. As such the electric current is: $\boldsymbol{I = \frac{V_{OC}}{R+R_L}}$, where R is the internal Resistance of the TE, and R_L is the load resistance. At maximum power, the resistances are matched and the current at maximum power becomes: $\boldsymbol{I_m = \frac{V_{OC}}{2R}}$, and thus, with $V_{OC} = 2s_T\Delta T = 2s_T(T_H - T_a)$, the maximum power that the TE generates is [26]:

$$\begin{aligned} P_m = V_m I_m &= \frac{V_{OC}}{2} I_m = \frac{1}{2}\frac{s_T^2}{\rho_T}\frac{A_L}{l}(T_H - T_a)^2 \\ &= \frac{1}{2}Zk_T\frac{A_L}{l}(T_H - T_a)^2 \end{aligned} \qquad (20)$$

Where Z is the thermoelectric material figure-of-merit ($s_T^2/\rho_T k_T$). Good typical values (Bi_2Te_3) are of the order of 0.003 K^{-1} while k_T is of the order of 1.7 W/m.K. Leg areas and lengths differ by design and typically for current designs they would be such that the rectangular leg has a side length of around 5 mm by 5 mm and a length (height) of about the same.

Equating Eqs. 18 and 19 and solving for T_p (=T_H) produces

$$\begin{aligned} T_H = {} & \frac{1}{3}T_a + \frac{4}{3Z}\left(\frac{BCG}{k/l} - \frac{h}{k/l} - 1\right) \\ & + \frac{4}{3Z}\sqrt{\frac{1}{4}Z^2T_a^2 + + \left(1 + \frac{h}{k/l}\right)^2 + \frac{1}{4}\left(5\left(1 + \frac{h}{k/l}\right) - \frac{BCG}{k/l}\right)ZT_a + \frac{BCG}{k/l}\left(\frac{BCG}{k/l} - 2\left(1 + \frac{h}{k/l}\right)\right) + \frac{3}{2}\frac{(1-A)CG}{k/l}Z} \end{aligned} \qquad (21)$$

The results of this section are only cosmetic and are only reported as a stepping stone to the next section. Some of the shortcomings of this sections assumption that T_L=T_a will be displayed flowingly and contrasted to more accurate results.

Realistic one–node PV-TE model

While providing simplicity and some insight, the previous treatment assumed T_L=T_a and hence gave very high outputs for the TE. The exercise is now repeated but with T_L not equal to T_a and governed by the heat balances at the TE's cold side. Hence, Equation I8 still represents the PV energy balance at the hot side, However, both equations 18 and 19 are modified by using T_L as the cold side temperature rather than T_a. Using the same reasoning as was associated with

Equation 18 and 19, the heat added from the PV to the hot side of the TE is:

$$\frac{\dot{Q}_H}{A_P} = \frac{s_T I T_H}{A_L} + \frac{k_T}{l}(T_H - T_L) - \frac{1}{2} I^2 \frac{2\rho_T l}{A_L^2} \quad (22)$$

Again, equating equations 18 and 22 gives;

$$\frac{3}{8}ZT_H^2 + \left(1 - \frac{BCG}{k/l} - \frac{h}{k/l}\right)T_H - \frac{1}{4}ZT_H T_L - \frac{1}{8}ZT_L^2 - T_L - \frac{(1-A)CG}{k/l} - \frac{h}{k/l}T_a = 0 \quad (23)$$

On the TE cold side:

$$\frac{\dot{Q}_C}{A_P} = \frac{s_T I T_L}{A_L} + \frac{k_T}{l}(T_H - T_L) + \frac{1}{2} I^2 \frac{2\rho_T l}{A_L^2} \quad (24)$$

Assuming the cold side of the TE is equipped with a heat sink of effectiveness ε gives the rate of heat removal at the heat sink below the TE cold side per PV area as (where h may represent some effective convection-radiation coefficient):

$$\frac{\dot{Q}_C}{A_P} = \varepsilon h(T_L - T_a) \quad (25)$$

Equating equations 24 and 25 provides:

$$\frac{1}{8}ZT_H^2 + T_H + \frac{1}{4}ZT_H T_C - \frac{3}{8}ZT_L^2 - \left(1 + \frac{\varepsilon h}{k/l}\right)T_L + \frac{\varepsilon h}{k/l}T_a = 0 \quad (26)$$

The resulting highly non-linear Equations 23 and 26 necessitate the use of a numerical solver. Therefore, parametric values that may be kept constant for certain cases are used. These include: Ambient temperature: T_a=20°C (293K), thermal conductivity of the thermoelectric material (Bi_2Te_3): k=1.7 W/m.K, thermoelectric leg length: l=0.005 m , surface heat transfer coefficient h=22 W/m²K, and the Shockley-Queisser efficiency coefficients for C-Si: A= $\eta_R(1 + \beta_R T_R)$ = 0.2595 and B= $\eta_R\beta_R$ = 0.000468K⁻¹.

The temperature of the PV panel (assumed equal to the TE hot side temperature) can be evaluated with this realistic model. Figure 8 shows the diminished rise in PV temperature due to TE bottoming for Z=0.003K⁻¹, ε=1 and Ta=293K with increasing insolation and augmentation by concentration. Included in the figure is the temperature of the PV that would result using the assumption that the cold side of the TE was somehow controlled at Ta. Hence that model (Equation 21) cannot be used as it grossly overestimated the resulting arrest in temperature rise due to TE bottoming of the PV.

Using the exact model, Figure 9 shows that for a given insolation the temperature of the hot side of the TE drops very slowly with improved thermoelectric-figure-of-merit and hence the PV efficiency tends to increase somewhat. Figure 9 further shows that the simpler assumption that assumes T_L=T_a grossly underestimates T_p at high insolation

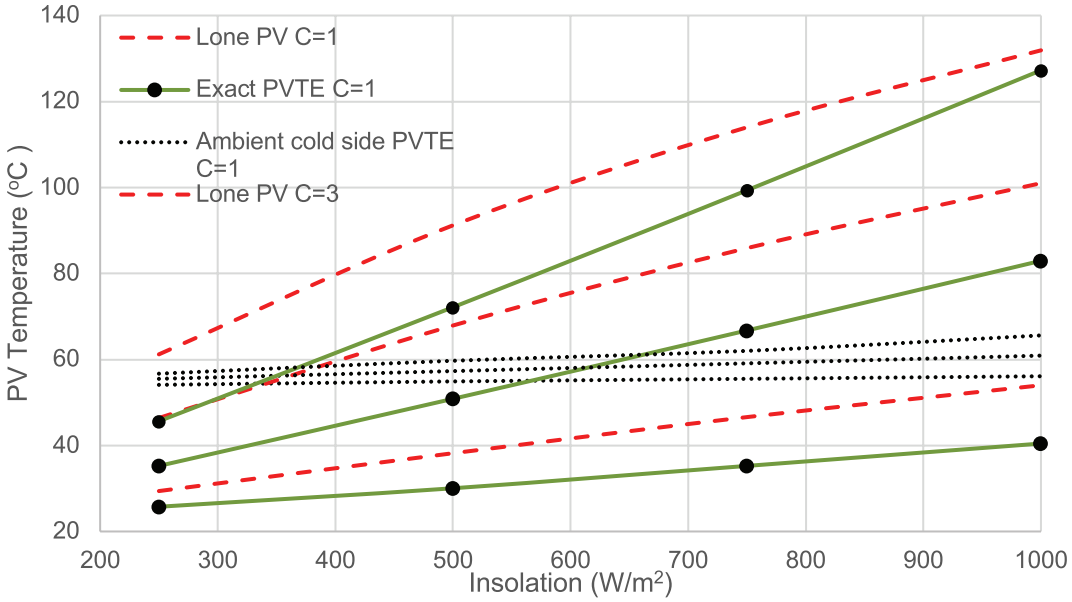

Figure 8. Demonstrating that the model assuming T_L=T_a cannot capture the effect of TE bottoming on the PV temperature.

but overestimates it at lower insolation's. All further discussions will use the exact model.

At lower solar insolation's with no further concentration, the difference between T_H and T_L is small as can be seen in Figure 10 which gives the temperature span (or swing) $\Delta T = T_H - T_L$ across the TE element at C=1 and ε=1 for several insolation's at 2 different thermoelectric-figures-of-merit. The span drops slightly with higher Z's but also increases slightly at higher insolation.

The TE heat sink effectiveness influences the magnitudes of the hot and cold side temperatures, but as Figure 11 shows (At G=1000 W/m² and C=8 – a high value!), the temperature swing (ΔT) across the TE drops slowly with Z and remains in the few degrees range and no more than 13K. The figure shows that with improved Z's the temperature swing actually is on a downward trend and this is not heat sink related. Unless the heat sink effectiveness is large (which usually requires external intervention), the temperature swing (ΔT) across the TE is small.

At an insolation of 1000 W/m², for concentrations of 1 or 3, the influence of the cold side heat-sink effectiveness as well as the thermoelectric-figure-of-merit are seen in Figure 12. As commented, the temperature swing across the TE is small and only reaches about 5 degrees at the higher concentration level of C=3. The temperature swing drop as the thermoelectric-figure-of-merit improves is clear. Apparently, the higher the Z, the better thermoelectric conversion of heat leaves less sensible internal energy increase.

For the typically available value of Z=0.003K^{-1}, at an insolation of 1000 W/m² and with an achievable heat sink

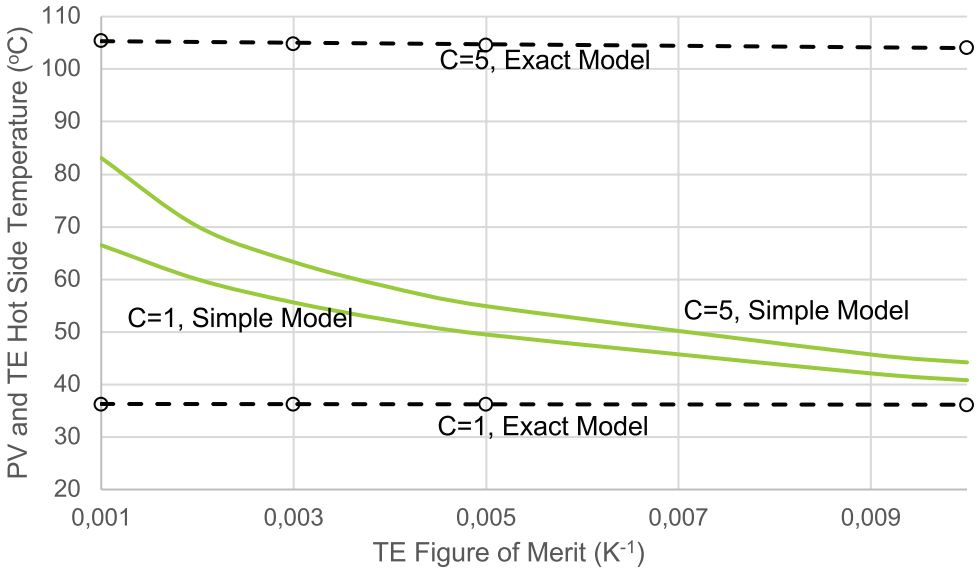

Figure 9. T_H (=T_P) as a function of Z for exact model vs. simpler model that assumed T_L=T_a. (C=1, ε=1, G=800 W/m²).

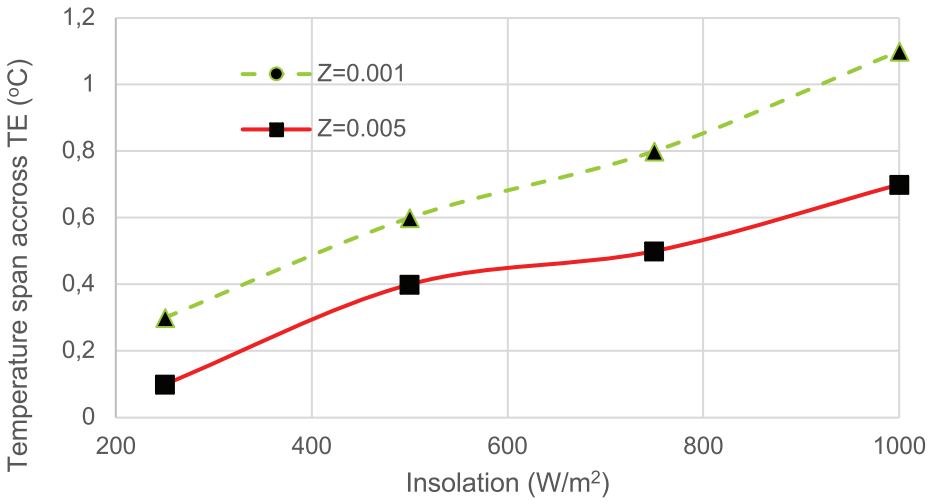

Figure 10. Temperature span (ΔT) across the TE element as a function of insolation.

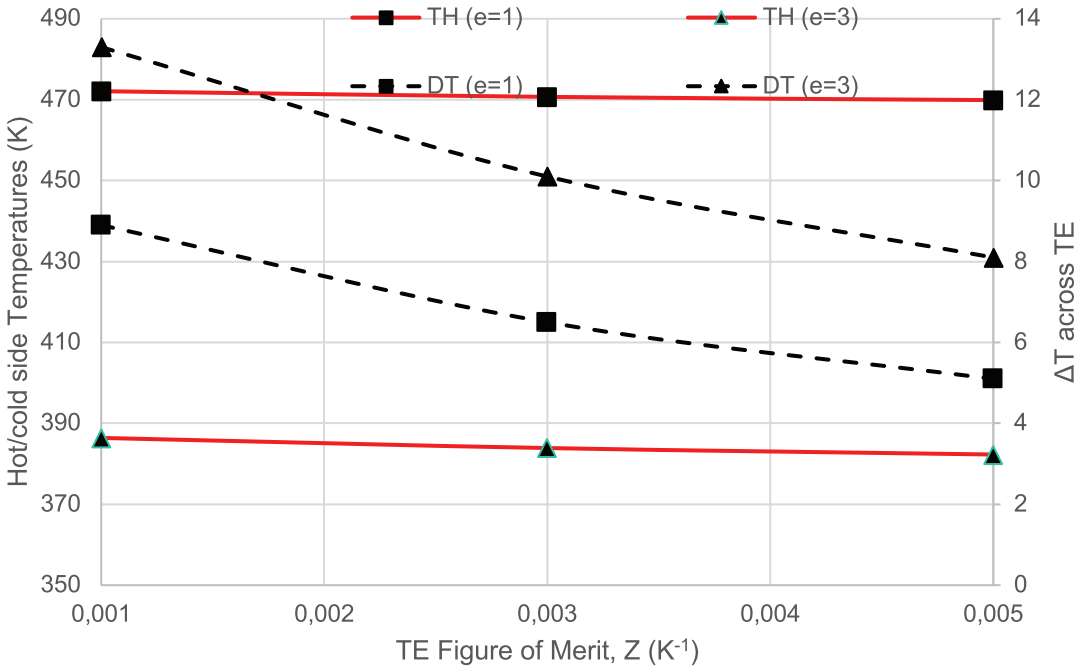

Figure 11. The effect of Z and ε on TE temperature swing (ΔT) at high concentration (C=8 at 1 sun).

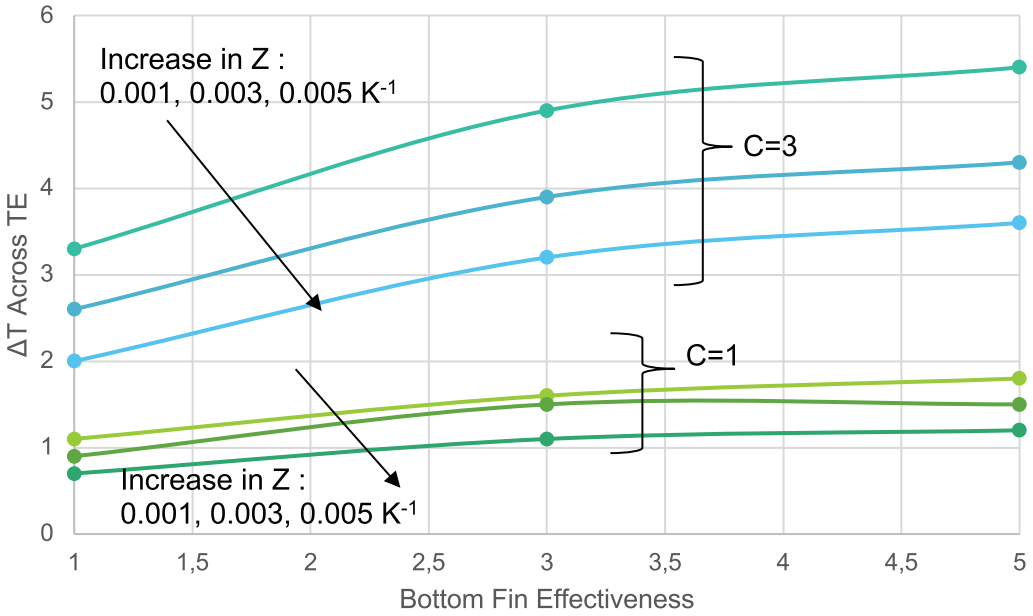

Figure 12. Temperature swing (span) (ΔT) across TE as a function of bottom fin effectiveness at G=1000 W/m² and 2 concentrations for different Z values.

effectiveness of ε=3, Figure 13 gives the TE max power contribution, the PV panel power contribution and the total power per unit panel area of the PV-TE hybrid for different solar concentrations. It is seen that the total power exhibits a maximum at about C=12. Beyond that, the rapid temperature-instigated deterioration in PV efficiency diminishes the supplementary increase in TE output. The concentration range displayed extends to the limit posed by Bi_2TE_3 material properties although there is an earlier lower limit posed by the PV material properties which further reduces the allowed concentration.

In fact, at the currently permissible concentrations of no more than 5, and with a temperature swing of no more than 6 degrees, the TE contributes about 4.15% of total power which at this level amounts to about 500 watts per unit area while the PV temperature is about 75°C. Hence, the added

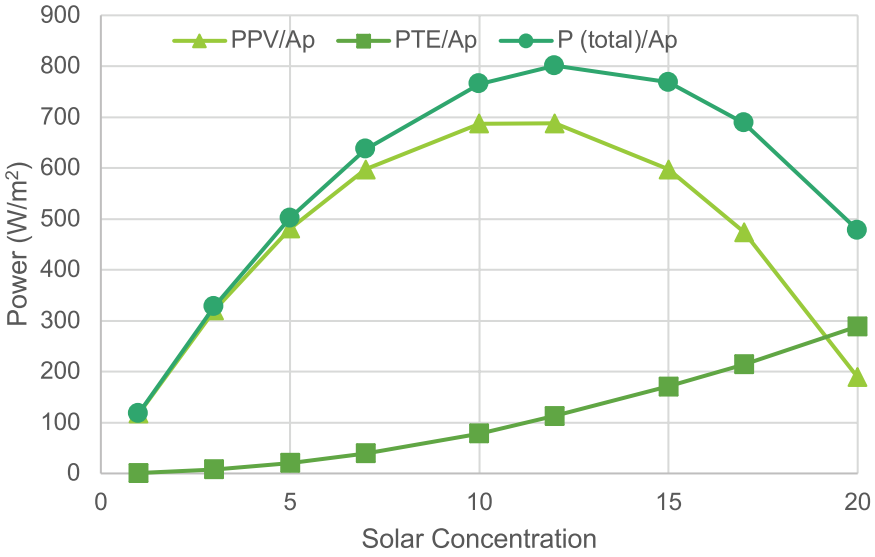

Figure 13. Specific power Contributions for a PV-TE combination at G=1000 W/m² at different concentrations.

value of the TE is not quite justifiable. It is also observed that PV and TE contributions are equal at a concentration of about C=18 (with G=1000 W/m², this is equivalent to 18 kW/m²) and total only about 275 W/m² which is about equal to the value at the feasible concentration level of C=3!

RESULTS AND DISCUSSION

As an initial effort, this work has shown that a simplified (properly averaged, 1-node model) for a photovoltaic slab can simplify determinations when more complex PV-TE hybrids are performed and produce reasonably accurate results that minimize unnecessary complications.

More significantly, for the PV-TE hybrid, the overall results of this study are very much in line with those Bjork and Nielsen [18] and other studies and appear to verify that TE bottoming of PV panels may not always be as attractive as is hoped for. At normal insolation's there is virtually no added benefit to bottoming the PV panel due to the very small temperature swing across the TE component. For example, at a concentration of C=1 (and G=1000 W/m²) and with an effectiveness of ε=3, it is seen that the TE component (at Z=0.003K^{-1}) produces 0.86 W/m² while the PV component effectively produces all the remaining 118 W/m² (i.e. less than 1%). A solitary PV panel at this insolation would be at a temperature of about 309K (note all comparisons with the solitary PV are based on the 1-node model) and would generate about 114 W/m² – this seems to indicate that the TE slab, at such a low insolation, behaves more like a passive thermal resistance.

The PV-TE hybrids maximum power production point is at a concentration of about 12 at an insolation of 1000 W/m², beyond which point, although the TE starts to contribute somewhat, the PV panel suffers significantly due to the temperature rise. At such an insolation level, the PV component with TE bottoming generates 600 W/m² out of a total 800 W/m² and is at a temperature of 159°C (which is clearly above its normal operating limit!). Had the PV panel been solitary, it would be at a temperature of about 209°C and would generate about 403 W/m². Thus, the value of TE bottoming is only apparent at higher insolation's as can be normally achieved by adding concentrating measures and equipment.

CONCLUSION

After establishing a simple, straightforward and clear methodology on the effect of temperature on PV panel performance, formulations were proposed to study the effect of bottoming the PV panel by heat engines. Starting the analysis by assuming bottoming with a hypothetical Carnot engine provides some simple insight into upper bound limitations. Furthermore, bottoming with an irreversible and hence realistically achievable thermoelectric generator showed some, albeit small, margin for performance enhancement. However, it emerges that adding a TE below the PV panel, while being quite an attractive and elegant option, cannot at the current technology state be thermally (or economically) justified unless the solar input is raised to levels wherein the PV panel becomes close to its upper material limit.

Henceforth, suggestions that claim large (more than 20%) enhancements in the output of thermally-in-series-connected PV-TE combinations – i.e. PV-TE hybrids, needs further scrutiny.

Hence, it is proposed that further research be geared towards high concentration physics. It remains to be seen if using higher temperature Thermoelectrics such as PbTe may increase the total output. For PbTe, while Z is somewhat less than for Bi_2Te_3 (around 0.001) it nevertheless peaks at about 300°C as opposed to around 150°C for the former.

Thus, the question remaining is whether the sacrifice in PV output due to higher temperature can be compensated by a larger conversion efficiency of the TE material. Further work on this line may include more TE material considerations, more rigorous heat sink treatment, and could the effect of further Tri-hybridization that includes PV-TE and TEC's thermally-connected I series.

NOMENCLATURE

C Solar concentration (≥1)
G Insolation (Solar Intensity), W/m^2K
h Convection heat Transfer coefficient, W/m^2K
T Temperature, °C (or K as required)
k Thermal conductivity, W/m °C (or W/m K)
A Area, m^2
l Thermoelectric leg length (height), m
Z Thermoelectric figure-of-merit, K^{-1}
s Thermoelectric Seebeck coefficient, V/K

Greek symbols
τ Solar transmission coefficient
α Solar Absorption coefficient
η Photovoltaic conversion efficiency
η_C Carnot efficiency, (% or fraction as indicated)
β_R Solar extinction or attenuation coefficient, m^{-1}
ε Heat sink effectiveness (≥1)
ρ Electric resistivity, Ohm.m

Subscripts
p Refers to photovoltaic
T Refers to thermoelectric
R Refers to reference value
a Refers to ambient
H Refers to hot side of thermoelectric
L Refers to cold side of thermoelectric

AUTHORSHIP CONTRIBUTIONS

Authors equally contributed to this work.

DATA AVAILABILITY STATEMENT

The authors confirm that the data that supports the findings of this study are available within the article. Raw data that support the finding of this study are available from the corresponding author, upon reasonable request.

CONFLICT OF INTEREST

The author declared no potential conflicts of interest with respect to the research, authorship, and/or publication of this article.

ETHICS

There are no ethical issues with the publication of this manuscript.

REFERENCES

[1] International Energy Agency (IEA). TCP PVPS Snapshot of Global PV Markets 2022. Report IEA-PVPS T1-42: 2022. Available at: https://iea-pvps.org/wp-content/uploads/2022/04/IEA_PVPS_Snapshot_2022-vF.pdf. Accessed Aug 14, 2024.

[2] Chavez-Erbiola EA, Vorobiev YuV, Bulat LP. Solar hybrid systems with thermoelectric generators. Sol Energy 2012;86:369-378. [CrossRef]

[3] Najafi H, Woodbury KA. Modeling and analysis of a combined photovoltaic-thermoelectric power generation system. J Sol Energy 2013;135:031013. [CrossRef]

[4] Kane A, Verma V. Performance enhancement of building integrated photovoltaic module using thermoelectric cooling. Int J Renew Energy Res 2013;3:320-324.

[5] Benghanem M, Al-Mashraqi AA, Daffallah KO. Performance of solar cells using thermoelectric modules in hot sites. Renew Energy 2016;89:51-59. [CrossRef]

[6] Hadi MA, Yeo KS, Rafideh P. Thermoelectric cooling for solar PV. AIP Conf Proc 2023;2643:040005.

[7] Kayabasi R, Kaya M. Effect of module temperature on module efficiency in photovoltaic modules and recovery of photovoltaic module heat by thermoelectric effect. J Therm Engineer 2023;9:191-204. [CrossRef]

[8] Sahin AZ, Ismaila KG, Yilbas BS, Al-Sharafi A. A review on the performance of photovoltaic/thermoelectric hybrid generators. Intl J Energy Res 2020;44:3365-3394. [CrossRef]

[9] Tyagi K, Gahtori B, Kumar S, Dhakate SR. Advances in solar thermoelectric and photovoltaic-thermoelectric systems for power generation. Sol Energy 2023;254:195-212. [CrossRef]

[10] Chandel R, Chandel SS, Prasad D, Dwivedi RP. Review on thermoelectric systems for enhancing photovoltaic power generation. Sustain Energy Technol Assess 2022;53:102585. [CrossRef]

[11] Kraemer D, Hu L, Muto A, Chen X, Chen G, Chiesa M. Photovoltaic-thermoelectric hybrid systems: A general optimization methodology. Appl Phys Lett 2008;92:243503. [CrossRef]

[12] Yonglian L, Witharana S, Cao H, Lasfargues M, Huang Y, Ding Y. Wide spectrum energy harvesting through an integrated photovoltaic and thermoelectric system. Particuol 2014;15:39-44. [CrossRef]

[13] Kandil AA, Awad MA, Sultan GI, Salem M. Performance of a PV/TE general hybrid system with a beam splitter under maximum operating conditions. Energ Conver Manage 2023;280:116795. [CrossRef]

[14] Von Sark WGJHM. Feasibility of photovoltaic-thermoelectric hybrid modules. Appl Energy 2011;88:2785-2790. [CrossRef]

[15] Park KT, Shin SM, Tazebay AS, Um HD, Jung JY, Jee SW, et al. Lossless hybridization between photovoltaic and thermoelectric devices. Sci Rep 2013;3:2123. [CrossRef]

[16] Lorenzi B, Mariani P, Reale A, Di Carlo A, Chen G, Narducci D. Practical development of efficient thermoelectric - Photovoltaic hybrid systems based on wide-gap solar cells. Appl Energy 2021;300:117343. [CrossRef]

[17] Bjork R, Nielsen KK. The performance of a combined solar photovoltaic (PV) and thermoelectric generator (TEG). Sol Energy 2015;120:187-194. [CrossRef]

[18] Bjork R, Nielsen KK. The maximum theoretical performance of unconcentrated solar photovoltaic and thermoelectric generator systems. Energ Conver Manage 2018;93:151-159.

[19] Wang N, Han L, He H, Park NH, Koumoto K. A novel high-performance photovoltaic-thermoelectric hybrid device. Energ Environ Sci 2011;4:3676-3679. [CrossRef]

[20] Lamba R, Kaushik SC. Modelling and performance analysis of a concentrated photovoltaic-thermoelectric hybrid power generation system. Energ Conver Manage 2016;115:288-298. [CrossRef]

[21] Chandan D, Arunachala, Varun K. Improved energy conversion of a photovoltaic module-thermoelectric generator hybrid system with different cooling techniques: Indoor and outdoor performance comparison. Int J Energy Res 2022;46:9498-520. [CrossRef]

[22] Yin E, Li Q. High efficiency dynamic lossless coupling of a spectrum splitting photovoltaic-thermoelectric system. Energy 2023;282:128294. [CrossRef]

[23] Shockley W, Queisser HJ. Detailed balance limit of efficiency of p-n junction solar cells. J Appl Phys 1961;32:510-519. [CrossRef]

[24] Skoplaki E, Palyvos J. On the temperature dependence of photovoltaic module electrical performance, a review of efficiency/power correlations. Sol Energy 2009;83:614-624. [CrossRef]

[25] Cengel Y, Boles M, Kanoglu M. Thermodynamics: An Engineering Approach. 9th ed. New York: McGraw Hill Education; 2018.

[26] Lee HS. Thermoelectrics: Design and Materials. New Jersey: John Wiley & Sons Ltd; 2017.